Proceedings of IMECE'03
2003 ASME International Mechanical Engineering Congress
Washington, D.C., November 15–21, 2003

IMECE2003-41574

FLUORESCENCE IMAGE RECONSTRUCTION FOR OPTICAL TOMOGRAPHY BASED ON TRANSIENT RADIATION TRANSFER EQUATION

Haiyong Quan and Zhixiong Guo*
Department of Mechanical and Aerospace Engineering
Rutgers, The State University of New Jersey, Piscataway, NJ 08854
***Corresponding Author: (732) 445-2024, guo@jove.rutgers.edu**

ABSTRACT

Image reconstruction is a bottleneck problem that impedes real time application of optical tomography technology. In this paper, we propose a novel fluorescence optical tomography method with a fast yet accurate algorithm for 3D image reconstruction. This imaging method is demonstrated using radiation transfer modeling based design. First the transport of ultrafast laser radiation governed by radiation transfer equation in participating media is simulated. Then the transient fluorescence field is obtained by solving the same radiation transfer equation in which the quantum yield of fluorescence is added to correlate the absorbed laser radiation with fluorescence emission intensity. Finally, 3D images are reconstructed using the temporal signals of fluorescence at detectors around the boundary of targeted tissues. We use the early time of fluorescence flight and the maximum fluorescence intensity to directly reconstruct the 3D images. Two new concepts, i.e., the photon migration statistic property and the solid geometric correlation property, are introduced for signal and image processing, respectively. The image reconstruction in this new method is very fast and does not require any inverse optimization. The accurate and efficient image and location of a $2.4\times2.4\times2.4mm^3$ tumor embedded at two different locations inside a $20\times20\times20mm^3$ rectangular tissue are demonstrated.

INTRODUCTION

In recent years, near-infrared (NIR) biomedical optical tomography (OT) is developing speedily. The non-invasive, safe, functional, and economical advantages allow OT to be a promising technique for supplementing and extending the using range of existing imaging modalities such as MRI and X-ray based CT. This technique employs NIR radiation measurements at the boundary of the highly scattering biological tissue to reconstruct the spatial distribution of optical properties of the target media [1-13]. In image reconstruction, most researchers used iterative methods to solve the inverse problem through a convergence algorithm of appropriate objective functions based on the forward modeling of either diffusion approximation equation (DAE) or radiative transfer equation (RTE). Hielscher's group [12,13], for example, used a gradient minimization algorithm to implement cross-sectional tomographic image using the time-independent RTE as the forward model. The majority of researchers in this field used the relatively simple DAE as the forward model. Among them, Jiang *et al*. [10,11] employed a finite-element solution of the Newton-type reconstruction algorithm to reconstruct the absorption and scattering coefficients of the heterogeneous turbid media using frequency-domain data. It is found that images from different modulation frequencies (from 50MHz to 300MHz) are almost no difference in visual content, but the higher contrast levels between the heterogeneous region and the background do exhibit more pronounced artifacts around the target boundary. Generally, the simulated or experimentally-measured signal information detected at the boundary just has low contrast information between the abnormal and normal tissues, especially when the abnormal tissue size is small. It's very difficult to let the objective function convergent and obtain clear images. The inverse problem is instable and morbid by nature, and may easily lead to divergence in the image reconstruction procedure. Moreover, it may take dozens of hours to reconstruct a tomographic image in conventional optical tomography methods although the diffusion approximation is adopted. Yet the quality and resolution of the images may still not be satisfied for clinical use [12]. To develop an effective, accurate and fast image reconstruction algorithm is of critical importance for achieving clinical application of OT technology.

To enhance and improve image contrast and quality appropriate fluorescence dyes may be introduced into the NIR

biomedical OT processes. The selective absorption property, amplified intensity signal-to-noise, and fluorescence spectrum and lifetime give us more information for image reconstruction. In fluorescence-based OT imaging, the solution of photon migration of both the excitation laser and fluorescence is coupled to obtain the fluorescence signals detected at the boundaries. In fluorescence image reconstruction, the iterative method, such as the conjugate gradient descent method and the simultaneous algebraic reconstruction technique [1-11], is still utilized to solve the inverse problem. For example, Chang *et al.* [2,3] reconstructed concentration and mean lifetime distributions in highly scattering media based on the analytic solution of the DAE and Monte Carlo simulation. Paithankar *et al.* [4] studied the feasibility of employing fluorescent contrast agents to perform optical imaging in tissue using fluorescence lifetime and yield information. Roy and Serick-Muraca [1] considered the inverse problem in a noncompressive geometry as a simple-bound constrained minimization problem in order to recover the interior fluorescence properties of exogenous contrast agent from frequency-domain photon migration measurements at the boundary. O'Leary *et al.* [6] formulated an inverse problem for fluorescence lifetime tomography. Li *et al.* [7] obtained analytic solutions of the infinite and semi-infinite homogeneous media or heterogeneous media containing a single spherical object using the DAE in the frequency-domain to determine the fluorophore lifetime and concentration changes. A three-dimensional Bayesian image reconstruction from sparse and noisy data sets is recently demonstrated by Eppstein e*t al.* [8]. Xu *et al.* [9] used the theory of the propagation of spatial Fourier components of the scattered wave field based on the DAE and a fast algorithm for three-dimensional reconstruction in a parallel planar geometry to reconstruct the layer maps of the absorption and scattering coefficients. Adding fluorescent dye into targeted tissue object amplifies the contrast between abnormal and normal tissues. In conventional image reconstruction, however, the solution of fluorescence radiation transfer must be coupled with the solution of the incident laser radiation transfer, and this leads to a more complicated iterative process in the inverse problem.

In this paper, we propose a novel optical imaging method using the time-domain parameters of fluorescence signals detected at the boundary. The time-resolved fluorescence signals are obtained by shining an ultrafast laser pulse to the target tissue embedded with a tumor where the fluorescent dye is concentrated. We will use the characteristics of ultrafast laser and fluorescence transport in tissues to directly reconstruct 3D images of the fluorescence emission which characterizes the shape, size and location of the tumor. This directly imaging process avoids the use of any inverse optimization and iteratively forward modeling. Its feasibility in locating and imaging small tumors will be demonstrated.

MATHEMATICAL MODELS

Governing Equations

The transport of laser excitation radiation and emitted fluorescence light is rigorously governed by the radiation transfer theory. The discrete ordinates method developed by our group [14] to solve the time-dependent radiation transfer equation incorporating radiation wave propagation with the

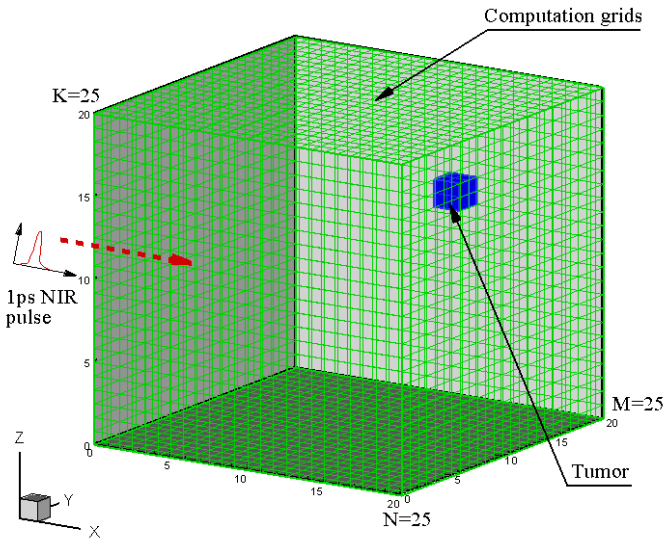

Figure 1. A 3D SIMULATION MODEL.

speed of light is employed to mimic the laser radiation and fluorescence transport. Figure1 illustrates a simulation model in which a 1 ps laser pulse is incident upon the wall at x = 0 in a cubic tissue phantom of 20×20×20mm^3 in size. A tumor-like object of 2.4×2.4×2.4mm^3 in size is embedded inside the phantom. The fluorescent dye is deposited uniformly in the tumor region. The fluorescent light excited by the incident pulse is received by detector arrays on the four side surfaces of the cubic tissue phantom. The detected fluorescence signals are time-resolved. The normal tissue phantom has an absorption coefficient σ_a=0.001 mm^{-1} and a scattering coefficient σ_s=1.0 mm^{-1}. In the tumor region, the absorption coefficient is larger because of the injection of fluorescent dye (σ_a=0.04 mm^{-1}). The transient radiative transfer equations in discrete ordinates form can be formulated as

$$\frac{1}{c}\frac{\partial I_i^l}{\partial t}+\xi^l\frac{\partial I_i^l}{\partial x}+\eta^l\frac{\partial I_i^l}{\partial y}+\mu^l\frac{\partial I_i^l}{\partial z}+\sigma_{ei}I_i^l=\sigma_{ei}S_i^l \qquad l=1,2,\ldots n \tag{1}$$

$$\frac{1}{c}\frac{\partial I_F^l}{\partial t}+\xi^l\frac{\partial I_F^l}{\partial x}+\eta^l\frac{\partial I_F^l}{\partial y}+\mu^l\frac{\partial I_F^l}{\partial z}+\sigma_{eF}I_F^l=\sigma_{eF}S_F^l \qquad l=1,2,\ldots n \tag{2}$$

where the subscripts i and F denote, respectively, the excitation laser and the consequent fluorescence light, ξ^l, η^l and μ^l are three direction cosines in a discrete ordinate direction $\hat{s}^l$, and σ_e is the extinction coefficient. The source terms S_i^l and S_F^l can be expressed as

$$S_i^l = \frac{\omega_i}{4\pi}\sum_{l'=1}^{n} w^{l'}\Phi^{l'l} I_i^{l'} + S_c^l \tag{3}$$

$$S_F^l = \frac{\omega_F}{4\pi}\sum_{l'=1}^{n} w^{l'}\Phi^{l'l} I_F^{l'} + \eta_F \frac{\sigma_{ai}}{4\pi\sigma_{eF}}\sum_{l'=1}^{n} w^{l'} I_i^{l'} \tag{4}$$

where $\Phi^{l'l}$ represents the scattering phase function $\Phi(\hat{s}^{l'} \rightarrow \hat{s}^{l})$, $S_c^{\,l}$ is the source contribution of the collimated laser irradiation, and η_F is the fluorescence quantum yield. The concentration variation of fluorescent dye is negligible in an ultrashort time period. The radiation transfer equations are solved with the discrete ordinates method [14]. A computational grid of 25×25×25 is used in simulation.

Signal Processing

When the incident NIR laser pulse irradiates the tumor region, fluorescent dye will be excited and emit fluorescence light. The fluorescence signals are received using fast photodiodes at the boundary of the tissue phantom. Figure 2 shows a typical fluorescence signal at a detector located at

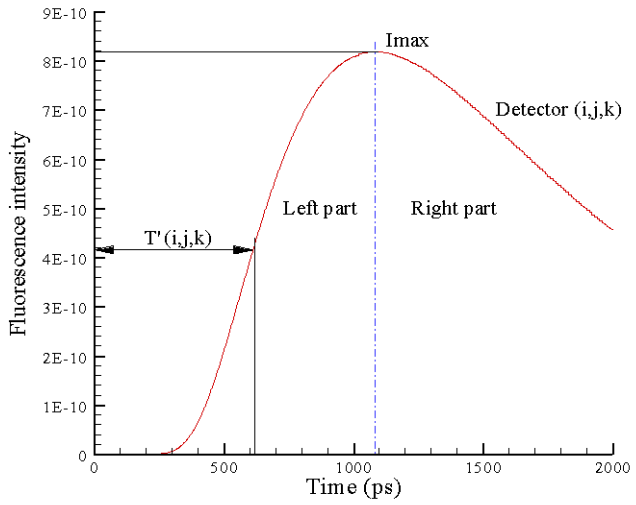

Figure 2. A REPRESENTATIVE FLUORESCENCE SIGNAL.

location (i,j,k). The maximum fluorescence intensity (MFI) is I_{max}. $T'_{i,j,k}$ is the flight time measured at half MFI and is defined as FTMHM. The indices of 'i', 'j' and 'k' indicate the sequence numbers of detector in the X, Y and Z directions, respectively. Let T'_{in} be the FTMHM from the detector at the laser incident position. The flight time of the earliest fluorescence from the tumor region to the detector (i, j, k) is then corrected as

$$T_{i,j,k}^F = T'_{i,j,k} - \frac{T'_{in}}{2.0} \tag{5}$$

Most fluorescence photons cannot travel in the tissue straightly to the boundary because its propagation is strongly interfered by the multiple scattering interactions. This results in a time delay in the detected earliest flight time. We hypothesize that the flight time of fluorescence photons is governed by a Gaussian probability distribution and $T^F_{i,j,k}$ is the mean value of the Gaussian probability distribution function. The probability of a specific fluorescence flight time is

$$P(T_{i,j,k}^C) = \frac{1}{\sqrt{2\pi}\sigma} e^{\frac{(T_{i,j,k}^C - T_{i,j,k}^F)^2}{2\sigma^2}} \tag{6}$$

where σ^2 is the variance of the data group of the flight times, and $T^C_{i,j,k}$ is the true flight time from the tumor region to the detector (i, j, k):

$$T_{i,j,k}^C = T_{i,j,k}^F - \sqrt{-2\sigma^2 \ln(\sqrt{2\pi}\sigma P(T_{i,j,k}^C))} \tag{7}$$

Equation (6) is called as the photon migration statistic property.

Image Reconstruction Algorithm

The average distance $R_{i,j,k}$ between the tumor and a detector located at (i, j, k) can be obtained as

$$R_{i,j,k} = T_{i,j,k}^C \frac{c_0}{n} \tag{8}$$

where c_0 is the speed of light in vacuum, and n is the refractive index of the tissue.

The equation for a spherical surface centered at the detector point (D_i,D_j,D_k) with a radius of $R_{i,j,k}$ is given by

$$(x - D_i)^2 + (y - D_j)^2 + (z - D_k)^2 = R_{i,j,k}{}^2 \tag{9}$$

We define a voxel space line as follows

$$x = V_{i'}, \qquad y = V_{j'} \tag{10}$$

and solve the intersection points between the spherical surface from formula (9) and the space line from formula (10). The voxel and pixel grid $(V_{i'},V_{j'},V_{k'})$ for imaging is finer than the computational grid in radiation transfer simulation. Figure 3 illustrates the distribution correlation between the pixel grid and computational grid.

When

$$R_{i,j,k}{}^2 - (V_{i'} - D_i)^2 - (V_{j'} - D_j)^2 \geq 0 \tag{11}$$

the intersection points can be located at

$$\begin{cases} V_{k'1} = D_k + \sqrt{R_{i,j,k}{}^2 - (V_{i'} - D_i)^2 - (V_{j'} - D_j)^2} \\ V_{k'2} = D_k - \sqrt{R_{i,j,k}{}^2 - (V_{i'} - D_i)^2 - (V_{j'} - D_j)^2} \end{cases} \tag{12}$$

If $$R_{i,j,k}{}^2 - (V_{i'} - D_i)^2 - (V_{j'} - D_j)^2 < 0 \tag{13}$$

there is no intersection point.

If $V_{k'1}$ and/or $V_{k'2}$ are located in the space of the tissue geometric model, the value of MFI received by this detector will be distributed to the voxel $(V_{i'},V_{j'},V_{k'})$ and its surrounding eight voxels. Repeating the same procedure for each detector, we can get the total intensity of each voxel contributed from all detector positions:

$$I(V_{i'},V_{j'},V_{k'}) = \frac{\left\{\begin{array}{l}\sum_{i=1}^{M}\sum_{k=1}^{K}\left[I_D(D_i,D_1,D_k;V_{i'},V_{j'},V_{k'}) + I_D(D_i,D_N,D_k;V_{i'},V_{j'},V_{k'})\right] \\ + \sum_{j=1}^{N}\sum_{k=1}^{K}\left[I_D(D_1,D_j,D_k;V_{i'},V_{j'},V_{k'}) + I_D(D_N,D_j,D_k;V_{i'},V_{j'},V_{k'})\right]\end{array}\right\}}{\left\{\begin{array}{l}\sum_{i=1}^{M}\sum_{k=1}^{K}\left[I_{MAX}(D_i,D_1,D_k) + I_{MAX}(D_i,D_N,D_k)\right] \\ + \sum_{j=1}^{N}\sum_{k=1}^{K}\left[I_{MAX}(D_1,D_j,D_k) + I_{MAX}(D_N,D_j,D_k)\right]\end{array}\right\}} \tag{14}$$

Here, $I(V_{i'},V_{j'},V_{k'})$ is the total dimensionless intensity of the voxel $(V_{i'},V_{j'},V_{k'})$, $I_D(D_i,D_j,D_k; V_{i'},V_{j'},V_{k'})$ is the intensity contributed from detector (D_i,D_j,D_k) to voxel $(V_{i'},V_{j'},V_{k'})$, and $I_{max}(D_i,D_j,D_k)$ is the maximum fluorescence intensity at detector position (i, j, k). We call the correlations from equation (8) to equation (14) as the solid geometric correlation property.

RESULTS

To demonstrate the feasibility of our new method, we apply the method to image and locate a small tumor embedded in a turbid tissue as shown in Fig. 1. Two cases are studied. In case A, the 2.4×2.4×2.4mm^3 tumor is located at the cubic center of (10, 10, 10) in the tissue phantom. In case B, the center of the 2.4×2.4×2.4mm^3 tumor is at location (15, 15, 15). We will reconstruct directly 3D images. Numerous tomographic images can be obtained from the 3D image. For the two cases studied, it took only four minutes in the 3D image reconstruction process in a Dell PC (Pentium 4, one CPU of 1.70 GHz, 512 MB DRAM). It is much faster than any reported OT methods. This fast and direct 3D image reconstruction is a unique feature of the present method. It will make real time clinical application possible.

Figure 4 shows the reconstructed 3D tumor image for case A. The blue block presents the tumor region. Initially we got a raw distribution of fluorescence intensity inside the tissue. Then a cutoff filtering technique is used to filter background noises and to enhance the signal/noise ratio and image contrast. The contrast-enhanced image in Fig. 4 gives clearly and accurately the shape and location of the embedded tumor at the center of the cubic tissue. The shape and size of the reconstructed tumor closely match to the original tumor shape

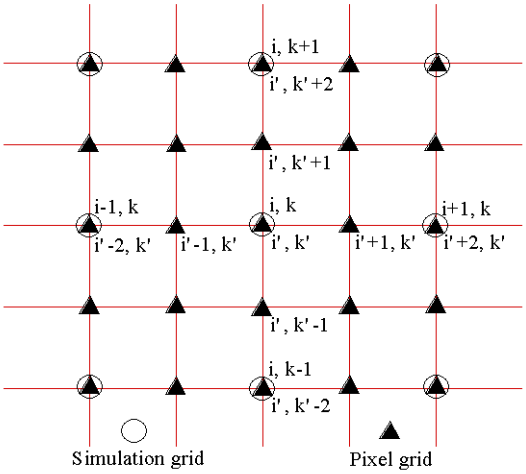

Figure 3. SKETCHES OF THE SIMULATION GRID AND THE PIXEL.

and size. The reconstructed tumor is located very closely to the center of the cube.

Figures 5a, 5b and 5c display the cross-sectional images for case A along the X, Y and Z directions, respectively. The shape, size and location of the tumor are visualized more clearly in each tomographic image than in the 3D image. The differentiation of fluorescence intensity possibility between the tumor region and surrounding area is very distinct. Here the deformation of the reconstructed images is clearly visible. Considering the facts that the tumor images are retrieved from a certain depth inside a turbid medium and that the tumor shape is very sharp, however, such a deformation is not surprising at all. The image quality is excellent and the contrast is very high. The tomographic images are very symmetric along the tumor central positions (Y = 10 mm or Z = 10mm) in the Y and Z directions as shown in Figs. 5b and 5c. However, the image location in the X direction slightly shifts to the small X direction in Fig. 5a. The central position in the reconstructed image is X = 9.1 mm, rather than X = 10mm. Such a 1 mm dislocation in the X direction can be attributed to the asymmetry of the simulated fluorescence signals detected at the walls of X = 0 and X = 20. Since the laser is incident from X = 0, the flight time detected at the wall of X = 0 is always smaller than that detected at the wall of X = 20 when the small tumor is

embedded at the center (X = 10). Such a dislocation may be overcome by shining lasers from several different locations.

The reconstructed 3D image for case B in which the tumor is centered at the location of (15, 15, 15) is shown in Fig. 6. Its tomographic images are shown in Figs 7a to 7c. The error of the tumor dislocation in this case is less than 0.5mm. The reconstructed images in the two exemplary cases have demonstrated the high accuracy, high contrast, and high image quality of the present imaging method.

CONCLUSION

We have developed and demonstrated a new imaging method for fluorescence optical imaging of small abnormal region in highly scattering turbid media. A fast and direct 3D image reconstruction is introduced in this new method. This 3D image reconstruction takes only several minutes and enables real time image processing for practical applications. The new concept of photon migration statistical property is introduced to correct the fluorescence flight time for fluorescence propagation in turbid medium. The solid geometric correlations are introduced to distribute the fluorescence signal intensities at the detectors to a spatial distribution of fluorescence possibility in the imaging voxel grid. The high possibility of fluorescence emission corresponds to an abnormal region.

The fluorescence signals are obtained through a radiation transfer modeling based design. The time-dependent radiation transfer and propagation of both the laser radiation and consequent fluorescence are solved with the discrete ordinates method. Such a modeling is accurate and can be used for practical fluorescence optical imaging design. A small tumor embedded at two different positions inside a 3D rectangular tissue is efficiently imaged and located using the proposed imaging method. The reconstructed tomographic images and 3D images are accurate with respect to the tumor shape, size and location. The reconstructed images are of high contrast and high quality. This new method has the potential to be developed into a diagnostic tool for early cancer detection and image.

REFERENCES

[1]Roy, R. and Sevick-Muraca, E.M., 2001. "Three-Dimensional Unconstrained and Constrained Image-reconstruction Techniques Applied to Fluorescence, Frequency-domain Photon Migration". Applied Optics, **40**(13), pp. 2206-2215.

[2]Das, B. B., Liu, Feng and Alfano, R. R., 1997. "Time-Resolved Fluorescence and Photon Migration Studies in Biomedical and Model Random Media". Report on Progress in Physics, **60**, pp. 227-292.

[3]Chang, J., Graber, H. L., Barbour, R. L.,1997. "Luminescence optical tomography of dense scattering media". Journal of Optical Society of American A, **14**(1), pp. 288-299.

[4]Chang, J., Graber, H. L., Barbour, R. L., 1997. "Imaging of Fluorescence in Highly Scattering Media". IEEE Transaction on Biomedical Engineering, **44**(9), pp. 810-822.

[5]Paithankar, D.Y., Chen, A. U., Pogue, B. W., Patterson, M. S., and Sevick-Muraca, E. M., 1997. "Imaging of Fluorescent Yield and Lifetime from Multiply Scattered Light Reemitted from Random Media". Applied Optics, **36**(10), pp. 2260-2272

[6]O'Leary, M. A., Boas, D. A., Li, X. D., Chance, B., and Yodh, A. G., 1996. "Fluorescence Lifetime Imaging in Turbid Media". Optics Letters, **21**(2), pp. 158-160.

[7]Li, X. D., O'leary, M. A., Boas, D. A., Chance, B., and Yodh, A.G., 1996. "Fluorescent Diffuse Photon Density Waves in Homogeneous and Heterogeneous Turbid Media: Analytic Solutions and Applications". Applied Optics, **35**(19), pp. 3746-3758.

[8]Eppstein, M. J., Hawrysz, D. J., Godavarty, A., and Sevick-Muraca, E. M., 2002. "Three-Dimensional Bayesian Image Reconstruction from Sparse and Noisy Data Sets: Near-infrared Fluorescence Tomography". PNAS, **99**(15), pp. 9619-9624.

[9] Xu, M., Lax, M., and Alfano, R. R., 2001. "Time-resolved Fourier optical diffuse tomography". Journal of Optical Society of American, **18**(7), pp1535-1542.

[10]Jiang, H., Xu, Y. and Iftimia, N.,2000. "Experimental Three-Dimensional Optical Image Reconstruction of Heterogeneous Turbid Media from Continuous-Wave Data". Optics Express, **7**(5), pp. 204-209.

[11]Jiang, H., Paulsen, K. D. and Osterberg, U., 1996. "Optical Image Reconstruction Using Frequency-domain Data: Simulation and Experiments". Journal of Optical Society of American A, **13**(2), pp. 253-266.

[12]Klose, A. D. and Hielscher, A. H., 2002. "Optical Tomography using the time-independent equation of radiative transfer—Part 2: Inverse Model". Journal of Quantitative Spectroscopy & Radiative Transfer, **72,** pp715-732.

[13]Hielscher, A. H., Klose, A. D. and Hanson, K. M., 1999. "Gradient-Based Iterative Image Reconstruction Scheme for Time-Resolved Optical Tomography". IEEE Transactions on Medical Imaging, **18**(3) pp. 262-271.

[14]Guo, Z. and Kumar, S., 2002. "Three-Dimensional Discrete Ordinates Method in Transient Radiation Transfer", Journal of Thermophysics and Heat Transfer, **16**(3), pp. 289-296.

[15]Bernd Jähne, 1997. *Digital Image Processing: Concepts, Algorithms, and Scientific Applications,* 4th ed., Springer-Verlag Berlin Heidelberg, New York, Chap. 8-9.

[16]M. Bertero and P. Boccacci, 1998. *Introduction to Inverse Problems in Imaging,* 1st ed., Institute of Physics Publishing, Bristol and Philadelphia

[17]K. R. Castleman, 1996. *Digital Image Processing,* 1st ed., Prentice-Hall International, Inc., New Jersey

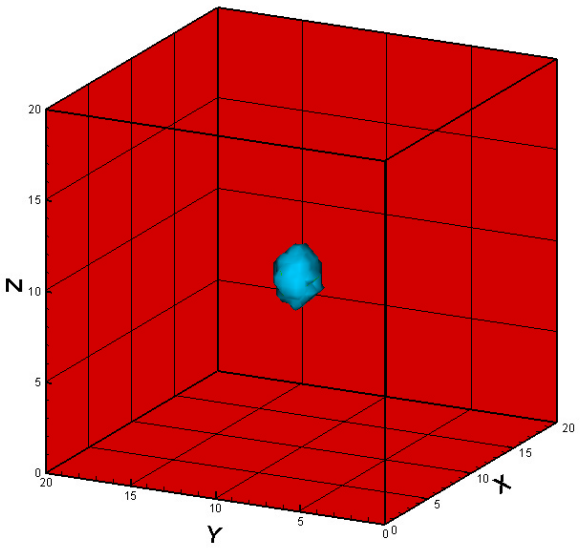

Figure 4. RECONSTRUCTED 3D TUMOR IMAGE FOR CASE A.

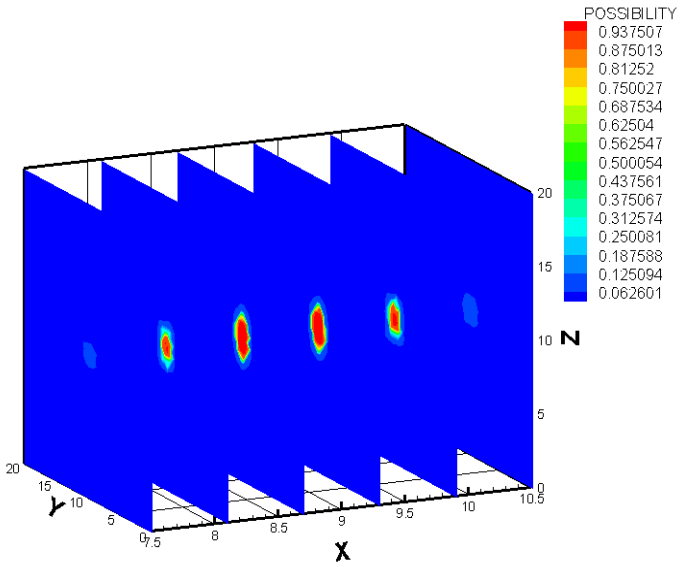

Figure 5a. TOMOGRAPHIC IMAGES IN Y-Z PLANE ALONG THE X DIRECTION.

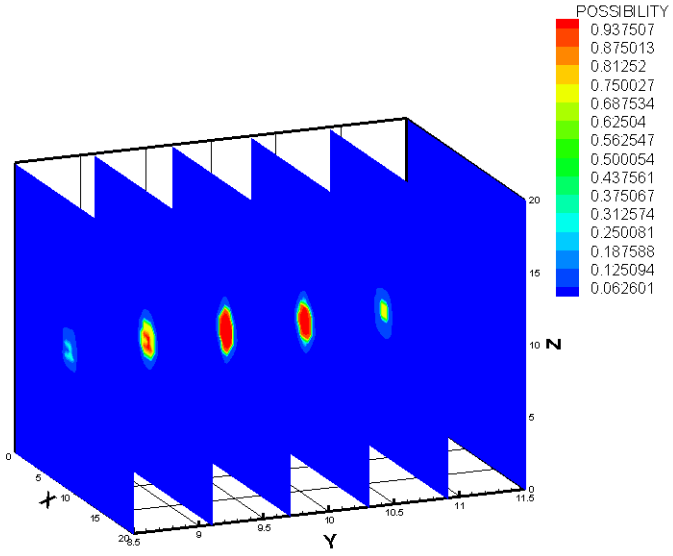

Figure 5b. TOMOGRAPHIC IMAGES IN X-Z PLANE ALONG THE Y DIRECTION.

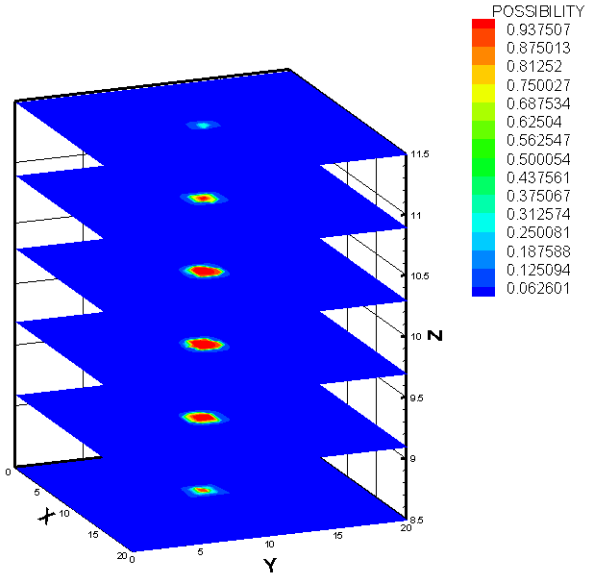

Figure 5c. TOMOGRAPHIC IMAGES IN X-Y PLANE ALONG THE Z DIRECTION.

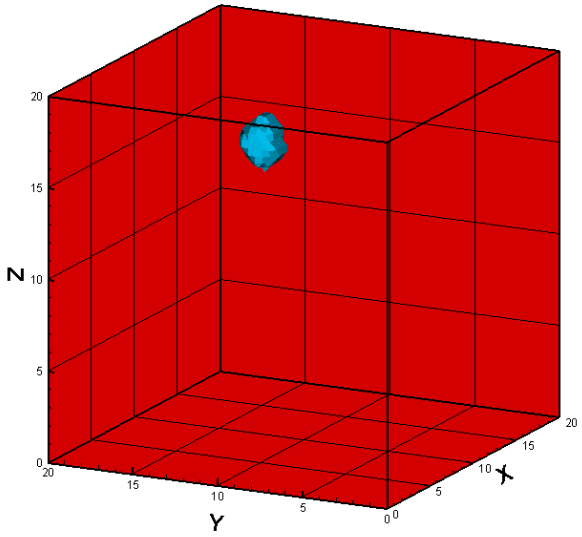

Figure 6. RECONSTRUCTED 3D TUMOR IMAGE FOR CASE B.

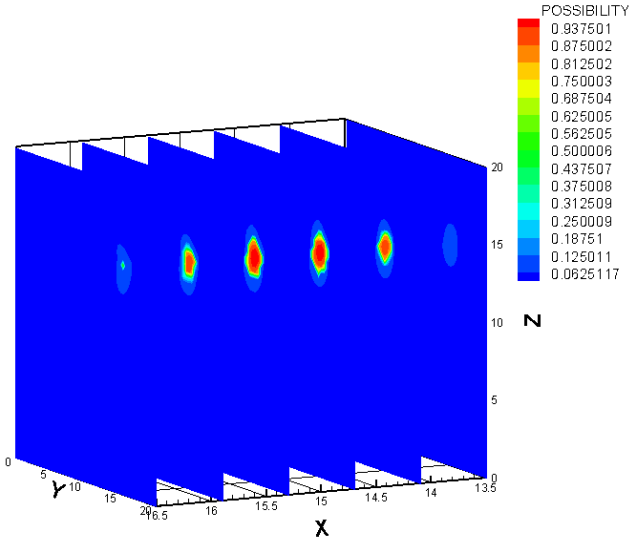

Figure 7a. TOMOGRAPHIC IMAGES IN Y-Z PLANE ALONG THE X DIRECTION.

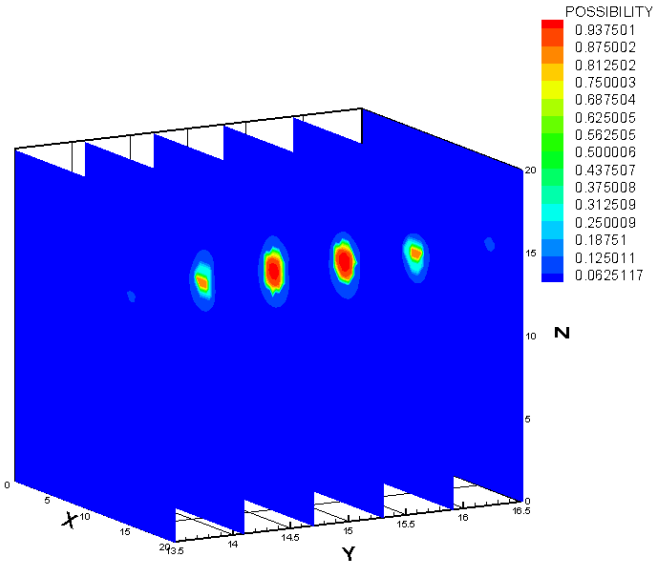

Figure 7b. TOMOGRAPHIC IMAGES IN X-Z PLANE ALONG THE Y DIRECTION.

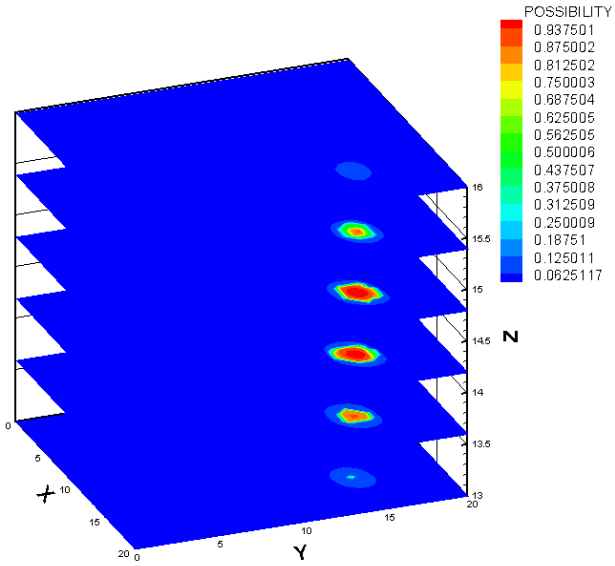

Figure 7c. TOMOGRAPHIC IMAGES IN X-Y PLANE ALONG THE Z DIRECTION.